Journal of Alloys and Compounds 527 (2012) 1–4

Contents lists available at SciVerse ScienceDirect

Journal of Alloys and Compounds

journal homepage: www.elsevier.com/locate/jallcom

Letter

Blue shift in band gap and photoluminescence of pulsed laser deposited SrS:Ce/quartz thin film nanophosphors

Ankush Vij[a,b], Sanjeev Gautam[a,b], Ravi Kumar[e], Amit K. Chawla[c], Ramesh Chandra[d], Nafa Singh[f], Keun Hwa Chae[a,*]

[a] Advanced Analysis Center, Korea Institute of Science and Technology, Seoul 136-791, Republic of Korea
[b] Pohang Light Source, San31 Hyojadong, Namgu, Pohang 790-784, Republic of Korea
[c] College of Engineering Studies, University of Petroleum and Energy Studies, Dehradun 248-007, India
[d] Institute Instrumentation Centre, Indian Institute of Technology, Roorkee 247-666, India
[e] Centre for Material Science and Engineering, National Institute of Technology, Hamirpur 177-005, India
[f] Department of Physics, Kurukshetra University Kurukshetra, Kurukshetra 136-119, India

ARTICLE INFO

Article history:
Received 12 October 2011
Received in revised form 7 February 2012
Accepted 8 February 2012
Available online xxx

Keywords:
SrS:Ce
Thin film nanophosphors
PLD
Photoluminescence

ABSTRACT

We report on the synthesis of single phase SrS:Ce/quartz thin film nanophosphors at a substrate temperature of 400 °C using pulsed laser deposition. The AFM and FESEM micrographs reveal the island structure with granular growth of nanophosphors. The average crystallite size (~ 13 nm using Williamson–Hall plot), the average grain size (~ 40 nm using AFM) and the blue shift in band gap confirm the nanostructure formation. Interestingly, the photoluminescence emission corresponding to $5d-4f$ transitions in Ce^{3+} ion under the cubic crystal field of SrS also exhibits a significant blue shift, which can be explained using phenomenological crystal field model modified by covalency factor.

© 2012 Elsevier B.V. All rights reserved.

1. Introduction

Rare earth ions doped alkaline earth sulfide (AES) phosphors are potential candidates for luminescent applications such as optical storage media, electroluminescent displays, radiation dosimetry, infrared sensors, ionoluminescence, etc. due to their high luminescence yields [1–5]. SrS, a member of AES family, acts as a good insulator due to indirect band gap of 4.2 eV in the bulk form. However, SrS doped with suitable activators such as rare earth ions exhibits excellent luminescent properties [6,7]. In addition, these phosphors emit visible light without self absorption.

Generally, thin film phosphors offer several advantages over the conventional powder phosphor screens, including high resolution, thermal stability, uniformity, density, and possibly a much lower susceptibility to charging [8]. There are several reports available on the synthesis of SrS based thin films on different substrates using pulsed laser deposition (PLD) [8,9], e-beam evaporation [10], RF sputtering [11], atomic layer epitaxy [12], etc. Since in low dimensional systems, electrons and holes are spatially confined causing quantum confinement effects, energy levels and hence optical properties become considerably different from their bulk counterparts [13–15]. This has generated a considerable interest in exploring nanomaterials both in powder [16–18] and thin film form [19–21]. Recently SrS based nanophosphors have been investigated in detail but only in their powder form [7,22,23]. In this letter, we discuss the hitherto unreported synthesis and characterization of SrS:Ce thin film nanophosphors. The effect of different substrate temperatures and subsequent in situ post deposition annealing on the structure of thin film nanophosphors has been investigated.

2. Experimental details

SrS:Ce thin film nanophosphors were deposited on quartz substrates using PLD. Prior to film deposition, substrates were properly cleaned in an ultrasonicator using methanol and deionized water. The source material Ce (0.5 mol%) doped SrS powder for PLD was synthesized by solid state diffusion method in the presence of thiosulfate as a flux [7]. The synthesized powder was hydraulically pressed into the pellet form and sintered at 1000 °C for 4 h in Ar atmosphere to prevent oxidation. The sintered pellet was used as the target to deposit thin films by using a PLD chamber (Excel instruments, Mumbai) and a KrF excimer laser (Lambda Physik, $\lambda = 248$ nm). The distance from target to substrate was fixed at 3 cm and the laser energy was adjusted at 250 mJ. The deposition was

* Corresponding author. Tel.: +82 542791192; fax: +82 542791599.
E-mail address: khchae@kist.re.kr (K.H. Chae).

0925-8388/$ – see front matter © 2012 Elsevier B.V. All rights reserved.
doi:10.1016/j.jallcom.2012.02.063

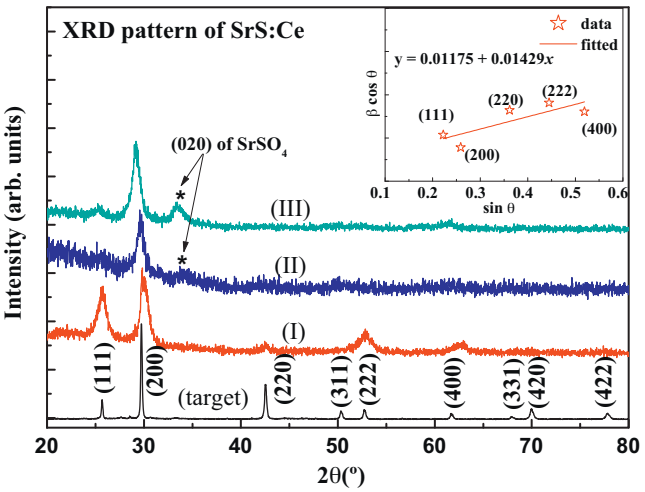

Fig. 1. X-ray diffraction pattern of SrS:Ce target and thin films deposited and subsequently in situ annealed for one hour at same temperature (I) 400 °C, (II) 500 °C (III) 600 °C. Inset shows the Williamson–Hall plot for single phase SrS:Ce thin film I. (For interpretation of the references to color in this figure legend, the reader is referred to the web version of the article.)

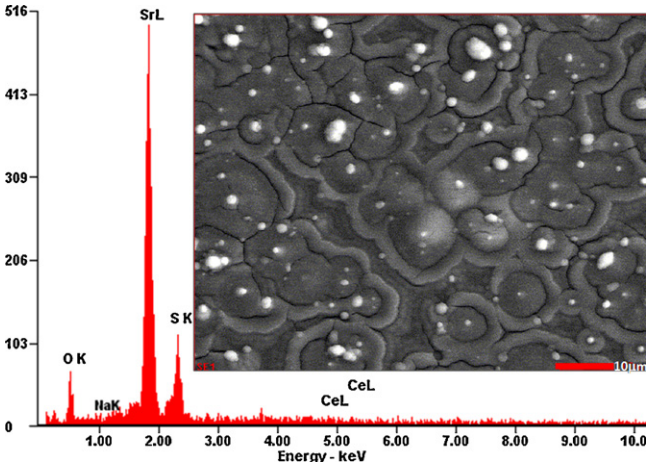

Fig. 2. The EDS spectrum and SEM micrograph of SrS:Ce thin film deposited at 400 °C. (For interpretation of the references to color in this figure legend, the reader is referred to the web version of the article.)

carried out under Ar partial pressure of 20 mTorr at a base pressure of 5×10^{-6} Torr. The thin film nanophosphors were deposited at different substrate temperatures of 400, 500 and 600 °C and subsequently in situ annealed at the substrate temperature for one hour and then allowed to cool in the presence of Ar environment. Hereafter, the films deposited and in situ annealed at 400, 500 and 600 °C will be referred to as thin film nanophosphors I, II and III respectively.

X-ray diffraction (XRD) was performed by using a Bruker's D8 Advance diffractometer (Cu K_α, 40 kV, 30 mA) in θ–2θ geometry. The UV–vis 2500PC double beam spectrophotometer (Shimadzu Corp., Japan) in the wavelength range of 190–900 nm was used for absorption spectroscopy. The surface morphology and compositional study were carried out using filed emission scanning electron microscopy (FESEM: FEI, Quanta 200F) equipped with electron dispersive spectrometer (EDS). The surface topography of the samples was investigated in tapping mode of atomic force microscopy (AFM), using a Nanoscope IIIa AFM system (Digital Instruments). He–Cd laser (325 nm) and a pre-configured Mechelle spectrograph were used to record photoluminescence (PL) emission spectrum.

3. Results and discussion

Fig. 1 shows the XRD pattern of SrS:Ce target and thin film nanophosphors I, II and III. The diffraction peaks of target can be indexed with standard JCPDS, No. 8-489 confirming the polycrystalline cubic rocksalt phase without any traces of impurity. All the thin films grown at different substrate temperatures also exhibit rocksalt cubic phase with a preferred orientation along (2 0 0), while other diffraction peaks almost disappear with the increase of substrate temperature. However, some minor secondary phase formation has also been observed for thin films II and III, possibly arising from $SrSO_4$ (0 2 0). It is apparent from the XRD that higher substrate temperature and subsequent in situ post deposition annealing cause a shift in 2θ towards lower diffraction angles with a small decrease in FWHM of the diffraction peaks. The preferred diffraction peak along (2 0 0) occurs at 2θ = 29.84°, 29.54°, 29.35° for thin film nanophosphors I, II and III. The lattice parameters corresponding to these 2θ values were calculated to be 5.980, 6.040 and 6.090 Å. The shift in diffraction angles to lower values can be associated with the increase of lattice parameter as a result of increasing substrate temperature. The XRD peaks in case of thin films are broadened appreciably as compared to target material itself indicating the decrease in grain size. Further characterization studies are restricted to the single phase thin film I only. The average crystallite size of thin film I has been calculated from FWHM of main diffraction peak using Debye Scherrer's equation [24]. The FWHM of any diffraction peak can be expressed as a linear combination of the contributions from the lattice strains and the small grain size, through the Williamson–Hall relation [25]:

$$\beta \cos\theta = \frac{\lambda}{D} + \eta \sin\theta, \tag{1}$$

where η is the effective strain, D the average crystallite size, λ the incident wavelength, θ the Bragg angle and β the diffracted FWHM (in radians) caused by the crystallites. The inset in Fig. 1 represents the Williamson–Hall plot of $\beta \cos\theta$ versus $\sin\theta$. The average crystallite size corresponding to zero strain is obtained from the Y-intercept and is found to be ~13 nm. The plot has a positive slope (inset in Fig. 1), indicating a tensile strain [14].

Fig. 2 shows the FESEM picture and EDS spectrum of thin film nanophosphors. FESEM clearly reveals the island structure with granular growth of nanophosphors. The EDS spectrum confirms the presence of Sr, S and Ce, however the deposited film is found to be sulfur deficient. In addition, some minor traces of oxygen and sodium have also been observed. The oxygen traces most probably arise from the adsorption of oxygen on the surface of thin film after exposure to air. The presence of Na in the thin film was expected and has been ascribed to the use of sodium thiosulfate during synthesis of SrS:Ce powder. Sodium thiosulfate (Na^+) was added as a charge compensator to overcome the charge mismatch of the trivalent cerium in SrS matrix. The thickness of the thin film was estimated to be around 200 nm using X-SEM (not shown here). Fig. 3 shows the 2D and 3D AFM images of the thin film nanophosphors. The average grain size estimated with AFM measurement is found to be ~ 40 nm, which is greater in size than estimated from XRD. This can be attributed to the granular structure formation. Moreover, size calculations using XRD give average over the whole thickness of the film. On the contrary, AFM estimates the size of grains close to the surface. The average roughness of the film was found to be ~6.5 nm.

The effect of nanostructure formation on the bandgap of the thin film nanophosphors has been investigated using UV–vis spectroscopy in absorption mode as shown in Fig. 4. The fundamental

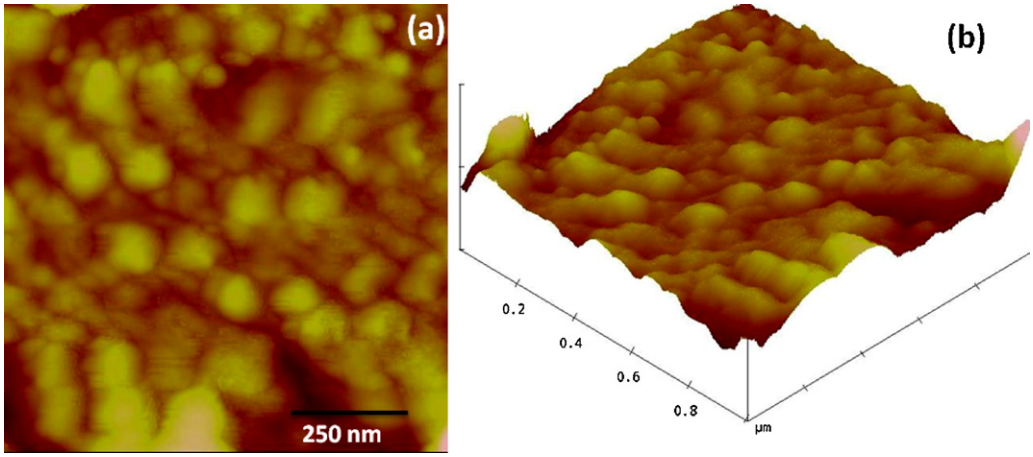

Fig. 3. (a) 2D AFM micrograph and (b) 3D AFM micrograph of SrS:Ce thin film deposited at 400 °C. (For interpretation of the references to color in this figure legend, the reader is referred to the web version of the article.)

absorption edge was used to calculate the optical band gap of the samples using the relation [26];

$$\alpha h\nu = (h\nu - E_g)^n \quad (2)$$

where $h\nu$ is the photon energy, α is the optical absorption coefficient near the fundamental absorption edge and n has a value of 1/2 for direct band gap and 2 for an indirect band gap. The absorption coefficient was calculated from the optical absorption spectra. Fig. 4 (a) shows the values of $(\alpha h\nu)^{1/2}$ for nanocrystalline SrS:Ce thin film plotted as a function of incident photon energy. The indirect band gap was obtained by extrapolating the linear portion of the graph and making $(\alpha h\nu)^{1/2} = 0$. The band gap of the thin film nanophosphors was calculated to be 4.52 eV, which is blue shifted in comparison to the band gap (~4.2 eV) of its bulk counterpart [7]. The blue shift in band gap is a clear signature of nanostructure formation [13,14] and may be attributed to the quantum size effect.

Fig. 4 (b) shows the PL spectrum of the thin film nanophosphors which comprises of a peak at 466 nm along with a shoulder around 515 nm. The emission bands at 466 and 515 nm may be assigned to the well known 5*d*–4*f* transitions of Ce^{3+} levels [7]. Since the 4*f* state of the Ce^{3+} ion is shielded from the influence of the surroundings, the crystal field of SrS causes only a small perturbation of the 4*f* state, which is negligible in comparison to the spin-orbit interaction. The spin-orbit interaction splits 4*f* levels into $^2F_{5/2}$ and $^2F_{7/2}$ levels. While the excited 5*d* levels being more sensitive to the crystal field of the host material, split into e_g and t_{2g} bands. Therefore, the PL emission at 466 nm with a shoulder at 515 nm may be attributed to the transitions from the lowest excited state $5d(t_{2g})$ to the ground state $4f(^2F_{5/2}, ^2F_{7/2})$ of Ce^{3+} ions in SrS. It is worth mentioning that PL emission in case of nanocrystalline thin film is significantly blue shifted than PL at 485 nm in case of microcrystalline thin film [11].

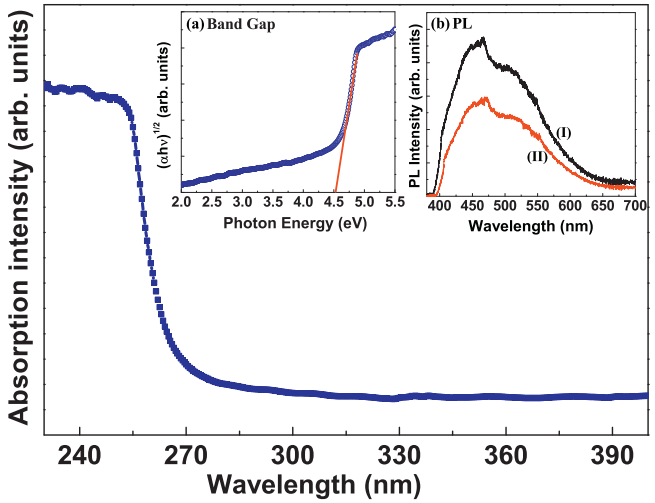

Fig. 4. Absorption spectrum of single phase SrS:Ce thin film I. Inset (a) shows the Tauc Plot for band gap determination and inset (b) shows the PL spectrum of SrS:Ce thin film I grown at 400 °C and thin film II grown at 500 °C. (For interpretation of the references to color in this figure legend, the reader is referred to the web version of the article.)

The PL spectrum of thin film II, with a relatively larger grain size has also been shown in Fig. 4 (b) for the comparison. It is clear that, apart from minor blue shift in emission wavelength, the PL output of nanocrystalline thin film I is almost 1.6 times higher than that from thin film II. We have also compared the PL spectrum of thin film nanophosphors with SrS:Ce powder phosphors reported elsewhere [7]. The blue shift in PL has been observed for SrS:Ce thin film nanophosphors, but the PL output was found to be almost six times lower than that from the powder phosphors. Huttl et al. [27] have also reported that PL yield for SrS:Ce,Cl thin films is around five times lower than that for powders.

Generally, the mechanism of luminescence in the semiconductor involves the recombination of electrons in the conduction band and holes in the valence band and shows a blue shift with the widening of band gap in nanomaterials due to quantum confinement. Since the luminescence in Ce doped SrS is due to the transition between energy levels of the dopant, the blue shift in PL can be explained on the basis of phenomenological crystal-field model modified by the covalency factor [28]. According to this model, the luminescence shift for Ce doped matrix depends on two parameters: the shift of energy centroid (E_c) in the 5*d* orbit and the effect of crystal field splitting. As the crystal size decreases to nanoscale, the bond distance between Ce^{3+} and the host matrix also decrease, which raises the centroid and t_{2g} energy levels. Consequently, the changes of energy levels in the centroid and t_{2g} shift the emission spectrum to shorter wavelength. Since pure SrS is a wide band gap material and does not show luminescence in visible region, hence PL spectroscopy also confirms the presence of Ce in SrS.

4. Conclusions

In conclusion, we have successfully synthesized single phase blue-luminescent SrS:Ce/quartz thin film nanophosphors at a

substrate temperature of 400 °C using pulsed laser deposition, which were subsequently in situ annealed at same temperature for 1 h in Ar environment. The average crystallite size using Williamson–Hall plot was calculated to be 13 nm. The FESEM and AFM reveal the island structure with granular growth of thin film nanophosphors with an average roughness of 6.5 nm. A blue shift in fundamental absorption edge of host matrix also confirms the nanostructure formation. Interestingly, PL emission at 466 nm and 515 nm, owing to 5*d*–4*f* transitions of Ce^{3+} levels, has also been found to be blue shifted as compared to its microcrystalline form. This blue shift in PL can be explained in the light of phenomenological crystal field model modified by covalency factor.

Acknowledgements

The authors are grateful to Korea Institute of Science and Technology (KIST) Seoul for providing financial assistance (KIST-2V02083) to support this research work.

References

[1] J.M. Fitz-Gerald, J. Hoekstra, P.D. Rack, J.D. Fowlkes, Appl. Phys. Lett. 82 (2003) 3466–3468.
[2] G. Sharma, A. Vij, S. Lochab, N. Singh, Appl. Surf. Sci. 257 (2011) 2764–2768.
[3] A. Piqué, R.C.Y. Auyeung, S.B. Qadri, H. Kim, B.L. Justus, A.L. Huston, Thin Solid Films 377-378 (2000) 803–808.
[4] A. Vij, S. Lochab, R. Kumar, N. Singh, J. Alloys Compd. 490 (2010) L33–L36.
[5] A. Vij, R. Kumar, F. Singh, N. Singh, A.I.P. Conf. Proc. 1349 (2011) 491–492.
[6] K. Korthout, P.F. Smet, D. Poelman, Appl. Phys. Lett. 98 (2011) 261919.
[7] A. Vij, S. Singh, R. Kumar, S.P. Lochab, V.V.S. Kumar, N. Singh, J. Phys. D: Appl. Phys. 42 (2009) 105103.
[8] C. Karner, P. Maguire, J. McLaughlin, S. Laverty, Philos. Mag. Lett. 76 (1997) 111–116.
[9] J.Y. Choe, S.M. Blomquist, D.C. Morton, Appl. Phys. Lett. 80 (2002) 4124–4126.
[10] P. Smet, D. Wauters, D. Poelman, R.L.V. Meirhaeghe, Solid State Commun. 118 (2001) 59–62.
[11] W.L. Warren, K. Vanheusden, D.R. Tallant, C.H. Seager, S.-S. Sun, D.R. Evans, W.M. Dennis, E. Soininen, J.A. Bullington, J. Appl. Phys. 82 (1997) 1812–1814.
[12] H. Heikkinen, L.-S. Johansson, E. Nykänen, L. Niinistö, Appl. Surf. Sci. 133 (1998) 205–212.
[13] R.N. Bhargava, D. Gallagher, X. Hong, A. Nurmikko, Phys. Rev. Lett. 72 (1994) 416–419.
[14] M.B. Sahana, C. Sudakar, G. Setzler, A. Dixit, J.S. Thakur, G. Lawes, R. Naik, V.M. Naik, P.P. Vaishnava, Appl. Phys. Lett. 93 (2008) 231909.
[15] V. Kumar, S.S. Pitale, V. Mishra, I. Nagpure, M. Biggs, O. Ntwaeaborwa, H. Swart, J. Alloys Compd. 492 (2010) L8–L12.
[16] S.K. Mishra, R.K. Srivastava, S. Prakash, R.S. Yadav, A. Panday, J. Alloys Compd. 513 (2012) 118–124.
[17] R.S.S. Saravanan, D. Pukazhselvan, C. Mahadevan, J. Alloys Compd. 517 (2012) 139–148.
[18] A. Vij, S. Lochab, S. Singh, R. Kumar, N. Singh, J. Alloys Compd. 486 (2009) 554–558.
[19] D. Beena, K. Lethy, R. Vinodkumar, A. Detty, V.M. Pillai, V. Ganesan, J. Alloys Compd. 489 (2010) 215–223.
[20] A.A. Ansari, S. Singh, B. Malhotra, J. Alloys Compd. 509 (2011) 262–265.
[21] H. Swart, O. Ntwaeaborwa, P. Nsimama, J. Terblans, Physica B, doi:10.1016/j.physb.2011.09.111, In press.
[22] V. Kumar, S.S. Pitale, M. Biggs, I. Nagpure, O. Ntwaeaborwa, H. Swart, Mater. Lett. 64 (2010) 752–754.
[23] E.I. Anila, A. Aravind, M.K. Jayaraj, Nanotechnology 19 (2008) 145604.
[24] B. Cullity, Elements of X-ray Diffraction, Addison-Wesley Publishing Company, Inc, London, 1996.
[25] S.B. Qadri, J.P. Yang, E.F. Skelton, B.R. Ratna, Appl. Phys. Lett. 70 (1997) 1020–1021.
[26] S. Sze, Physics of Semiconductor Devices, Wiley, New York, 2004, p. 39.
[27] B. Huttl, U. Troppenz, K.O. Velthaus, C.R. Ronda, R.H. Mauch, J. Appl. Phys. 78 (1995) 7282–7288.
[28] S. Mhin, J. Ryu, K. Kim, G. Park, H. Ryu, K. Shim, T. Sasaki, N. Koshizaki, Nano Res. Lett. 4 (2009) 888–895.